processes

MDPI

Article

Optimal Scheduling Method of Combined Wind–Photovoltaic–Pumped Storage System Based on Improved Bat Algorithm

Hui Fan [1,*], Hongbo Wu [1], Shilin Li [1], Shengfeng Han [2], Jingtao Ren [2], Shuo Huang [3] and Hongbo Zou [4,*]

[1] State Grid Hebei Electric Power Co., Ltd., Shijiazhuang 050081, China; wuhb@he.sgcc.com.cn (H.W.); lisl@he.sgcc.com.cn (S.L.)
[2] State Grid Xingtai Power Supply Co., Ltd., Xingtai 054001, China; yudjjfyg89464@163.com (S.H.); rjt2024@163.com (J.R.)
[3] Hubei Engineering and Technology Research Center for AC/DC Intelligent Distribution Network, School of Electrical Engineering and Automation, Wuhan University, Wuhan 430072, China; 18579255787@163.com
[4] College of Electrical Engineering and New Energy, China Three Gorges University, Yichang 443002, China
* Correspondence: px_fanh@he.sgcc.com.cn (H.F.); zhbhorace@ctgu.edu.cn (H.Z.)

Abstract: Pumped storage power stations not only serve as a special power load but also store excess electricity from the power system, significantly reducing the curtailment of wind and solar power. This dual function ensures the stable operation of the power grid and enhances its economic benefits. The scheduling optimization problem of a combined wind–solar–pumped storage system is addressed in this study, and an optimization scheduling model is proposed with the objective of maximizing total system revenue. The model is designed to comprehensively account for the generation revenues from wind power, photovoltaic power, thermal power, and pumped storage, as well as the penalty costs associated with pollutant emissions. To address the limitations of traditional algorithms, which are prone to being trapped in local optima and exhibit slow convergence, an improved bat algorithm was developed. The algorithm is enhanced through the use of chaotic mapping to expand the initial solution space, the incorporation of adaptive step-size updates to improve convergence efficiency, and the integration of the Cauchy function to strengthen global search capabilities, thereby effectively avoiding local optima. Simulation results have demonstrated that the improved algorithm achieves significant improvements over traditional bat algorithms and particle swarm optimization (PSO) in terms of optimization efficiency, with total revenue increases of 21.9% and 24.6%, respectively. The optimized scheduling plan is shown to fully utilize the flexible regulation capabilities of pumped storage, mitigating the adverse effects of wind and photovoltaic output fluctuations on grid operations and achieving a balanced trade-off between economic and environmental objectives.

Keywords: renewable energy systems; wind–photovoltaic–pumped storage; optimal scheduling method; improved bat algorithm

check for updates

Academic Editor: Krzysztof Rogowski

Received: 11 November 2024
Revised: 7 December 2024
Accepted: 11 December 2024
Published: 3 January 2025

Citation: Fan, H.; Wu, H.; Li, S.; Han, S.; Ren, J.; Huang, S.; Zou, H. Optimal Scheduling Method of Combined Wind–Photovoltaic–Pumped Storage System Based on Improved Bat Algorithm. *Processes* **2025**, *13*, 101. https://doi.org/10.3390/pr13010101

Copyright: © 2025 by the authors. Licensee MDPI, Basel, Switzerland. This article is an open access article distributed under the terms and conditions of the Creative Commons Attribution (CC BY) license (https://creativecommons.org/licenses/by/4.0/).

1. Introduction

With the global intensification of energy shortages and environmental pollution, the utilization of new clean energy to replace traditional fossil fuels for power generation has become the primary focus of the energy revolution. As a result, new energy power generation has emerged as a crucial component of the power system [1,2]. In recent years, the development of wind power and photovoltaic power generation has accelerated, making these forms of energy the mainstream of renewable clean energy, with steadily

increasing installed capacity and power generation. However, the uncertainty of output from new energy sources significantly affects the safe and stable operation of the power system [3,4]. To effectively utilize photovoltaic and wind power resources and advance energy transformation and green development, pumped storage power stations are widely recognized as an effective energy storage solution globally [5]. Therefore, studying a joint system dispatch method that integrates wind power, photovoltaic, thermal power units, and pumped storage units is of great significance for enhancing the absorption of new energy.

Numerous studies have investigated the impact of photovoltaic and wind power generation on peak shaving in power systems. It is generally agreed in the existing literature that wind power exhibits a significant inverse peak shaving characteristic throughout the day. During low-load periods, high wind power levels can cause the system's load to drop below its minimum output level, which may necessitate curtailing wind power or shutting down generation units [6]. On the other hand, photovoltaic power generation typically reaches its peak output around midday, but its output is nearly zero in the early morning and late evening, thus failing to meet the load demand during evening peak hours. Moreover, photovoltaic generation is highly sensitive to ambient temperature and light intensity, making it prone to drastic fluctuations and substantial drops in output [7,8]. Given these characteristics, the integration of photovoltaic and wind power into the power grid can negatively affect the power system's peak shaving operation. If the variation patterns during peak and off-peak hours are not properly addressed, a large portion of photovoltaic and wind turbines may be disconnected from the grid during these periods, leading to significant resource waste [9–12]. While there is some degree of temporal and spatial complementarity between photovoltaic and wind power generation, the in-depth research on this aspect remains insufficient.

Energy storage systems are flexible resources with excellent regulation capabilities, functioning as both power sources and loads. They are among the primary resources for peak shaving and smoothing power generation curves in power systems. Additionally, research on their applications has rapidly increased in recent years. M. S. Fakhar proposes a new model for accommodating wind power output, designing a case system for a wind-pumped storage combined system based on the actual parameters of a pumped storage power station [13]. The experimental results of the case system show that coordination between the pumped storage power station and the wind farm can significantly mitigate the adverse effects of the randomness of wind power output and substantially improve overall economic benefits. J. Li, et al. propose a joint operation system model for pumped storage and wind power generation, aiming to minimize operating costs when wind power levels are at their lowest [14]. Although Y. Lu et al. study the peak shaving role of energy storage in a combined wind–photovoltaic–storage system, they do not conduct an in-depth analysis of the impact of energy storage systems on peak shaving and renewable energy integration mechanisms [15]. Z. A. Khan, et al. establish a dynamic optimization dispatch model for a combined wind farm and pumped storage power station system with the goals of energy conservation and emission reduction [16]. This model fully considers various constraints and introduces two continuous variables, generation power and pumping power, to describe the operating characteristics of the pumped storage unit. Simulation results indicate that this method can achieve an optimal compromise between safety, economy, and environmental protection, thereby mitigating the impact of wind power output randomness. However, this model is overly complex and difficult to solve.

Modern heuristic optimization algorithms are powerful and effective tools for solving ill-conditioned optimization problems and have been widely applied in the field of power system optimization [17]. A complementary generation management strategy for wind–

photovoltaic–storage systems is proposed by M. Chazarra, et al. which takes into account the impact of battery charging and discharging depth and frequency on battery life. This strategy establishes a micro-grid cost model and employs the traditional PSO algorithm to solve it. L. Bao, et al. focus on optimizing the daily dispatch of distributed power sources from the perspective of optimal energy management by incorporating energy storage charging and discharging constraints and minimizing operating costs as the objective function [18]. The PSO algorithm is utilized to determine the optimal output for distributed power sources. L. Yang, et al. present a hybrid bat algorithm-based scheduling method for high-penetration wind power systems [19]. This method integrates wind curtailment penalty costs into the model, enhancing the scheduling model's adaptability to high-penetration wind power integration. While the method can effectively improve the solution efficiency for combined units, its scheduling accuracy remains relatively low. However, the aforementioned studies primarily consider either local or global search capabilities of the model's solution algorithms, leading to relatively low computational accuracy and an inability to achieve global optimal scheduling [20–22].

To address the limitations of traditional algorithms in handling the complexity of the current combined wind–photovoltaic–pumped storage system model, as well as the increasing dimensionality of optimal solutions in practical applications, and the convergence and optimization challenges of existing algorithms, an improved bat algorithm is proposed in this paper to solve the scheduling model of the combined wind–photovoltaic–pumped storage system. A comparative table with an analysis of this paper and previous studies is shown in Table 1. The contributions of this paper are as follows:

Table 1. The comparative table with an analysis of this paper with previous studies.

Study	Research Objectives	Optimization Methods	Application Scenarios	Algorithm Performance
M. S. Fakhar [14]	Optimize the economic and environmental performance of the wind–solar–pumped storage system	Multi-objective optimization based on particle swarm optimization (PSO)	Simulated wind–solar–storage system	Standard PSO algorithm, slower convergence, prone to local optima.
E. I. Ogunwole and S. Krishnamurthy [23]	Improve power generation scheduling of wind and photovoltaic and system stability	Hybrid genetic algorithm (GA) and PSO	Region with high penetration of wind and solar energy	Complex hybrid algorithm with limited applicability, no optimization for pollutant emission.
Y. Li, Z. Xie, S. Yang and Z. Ren [10]	Multi-objective scheduling optimization for wind–solar–pumped storage combined system	Multi-objective genetic algorithm (MOGA)	Real-world power grid in a specific region	Traditional algorithm, lacks optimization for escaping local optima, slower convergence.
This Study	Maximize total revenue of wind–solar–pumped storage system while considering pollutant emission penalties	Improved bat algorithm (with chaotic mapping, adaptive step size, and Cauchy function)	Practical scheduling scenario for combined wind–solar–storage systems	Improved bat algorithm significantly enhances convergence speed and global search ability, avoiding local optima.

(1) A comprehensive revenue-maximization scheduling optimization model was developed. An optimization scheduling model was proposed, which comprehensively considers the generation revenues from wind power, photovoltaic power, thermal power, and pumped storage, as well as the penalty costs for pollutant emissions. The model was designed to balance the overall system benefits in terms of both economic performance and environmental protection.

(2) An improved bat algorithm-based optimization method was designed and developed. The population initialization was performed using chaotic mapping to expand the coverage of the solution space. An adaptive step-size updating strategy was introduced to improve the convergence efficiency of the algorithm. Furthermore, the global search capability was enhanced by incorporating the Cauchy function, which prevents the algorithm from falling into local optima. These improvements resulted in higher efficiency and accuracy in solving complex optimization problems.

(3) The effectiveness of the model and algorithm combination was thoroughly validated. Through comparisons with traditional bat algorithms and particle swarm optimization (PSO), significant advantages were demonstrated by the improved algorithm in terms of convergence speed, optimization accuracy, and overall revenue enhancement. Experimental results confirmed that the improved algorithm is highly effective and superior for solving the combined scheduling problem, leading to a significant increase in both system stability and economic benefits.

The structure of this paper is organized as follows: Section 2 introduces the distributed combined generation system with pumped storage; Section 3 describes the wind–photovoltaic–pumped storage combined power generation scheduling model; Section 4 introduces the scheduling model solution method based on the improved bat algorithm; Section 5 presents the simulation verification; and Section 6 concludes this paper.

2. The Wind–Photovoltaic–Pumped Storage Combined System

Pumped storage power stations utilize the excess power of the power grid to drive the water pumps. The pumps draw water from the lower reservoir to the upper reservoir, converting electric energy into potential energy stored in the water of the upper reservoir. When the power supply of the grid is insufficient, the potential energy of the water is converted into electric energy through the hydroelectric generators. As an effective method of energy storage, pumped storage can effectively regulate the dynamic balance between the production, supply, and consumption of the power system [24,25].

The integration of pumped storage power stations can, to a certain extent, control the charging and discharging process based on the needs of the power grid, thus forming an integrated wind–photovoltaic–storage system. In the integrated wind–photovoltaic–storage system, the platform control mode is more convenient and flexible, and tends to become more intelligent with the development of technology. The platform control mode can adjust the role of the energy storage system based on the power load conditions. A typical integrated wind–photovoltaic–storage system platform mainly includes wind farms, photovoltaic arrays, energy storage systems, control centers, power transmission lines, signal feedback lines, etc. The system structure is shown in Figure 1.

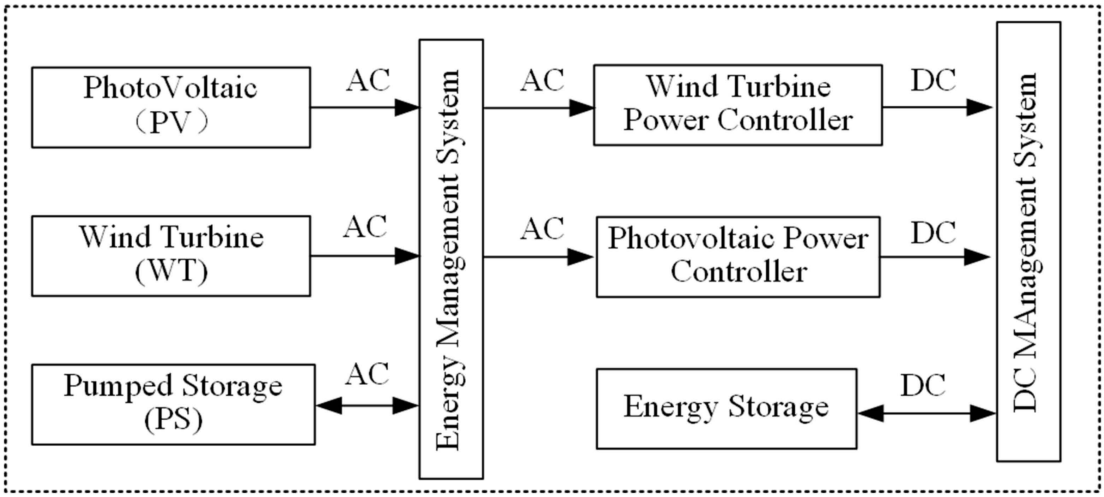


Figure 1. Power generation system for co-generation system with pumped storage.

The main components of a pumped storage power station are water pumps and turbines. During low-load periods, the water pumps draw water from the lower reservoir to the upper reservoir, converting excess electric energy from the grid into potential energy for storage. During peak load periods, the pumped storage power station directs water from the upper reservoir to the lower reservoir, driving the turbine generators in the main plant to generate electricity, converting potential energy into electric energy. The mathematical model for the energy storage and release processes of the pumped storage power station can be expressed as follows [6]:

$$P_{\mathrm{ps}}(t) = \frac{\rho_{\mathrm{w}} g H Q_{\mathrm{ps}}}{\eta_{\mathrm{p-m}}} \tag{1}$$

$$P_{pump}(t) = \rho_{\mathrm{w}} g H Q_{\mathrm{t}} \eta_{\mathrm{t}} \tag{2}$$

where $P_{\mathrm{ps}}(t)$ is the power of the pump; ρ_{w} is the density of the water; g is the acceleration of gravity; H is the pressure head of the pump; Q_{ps} is the volumetric flow of the water pumped to the reservoir; $\eta_{\mathrm{p-m}}$ is the efficiency of the pump; $P_{pump}(t)$ is the power generated by the turbine; Q_{t} is the volumetric flow of the water from the reservoir to the turbine; and η_{t} is the efficiency of the turbine.

The efficiency of pumped storage is affected by various loss mechanisms, including thermal losses in the hydraulic system and electrical losses in the generator and motor. The thermal losses in a pumped storage system primarily stem from the energy conversion process within the hydraulic system. These losses can be expressed through the efficiency of the pumps and turbines [26].

$$\eta_{\mathrm{pump}} = \frac{P_{\mathrm{hydraulic}}}{P_{\mathrm{input}}} \tag{3}$$

$$\eta_{\mathrm{turbine}} = \frac{P_{\mathrm{output}}}{P_{\mathrm{hydraulic}}} \tag{4}$$

where $P_{\mathrm{hydraulic}}$ represents the hydraulic power after the pump converts electrical energy into the potential energy of water; P_{input} denotes the input power to the pump; and P_{output} refers to the output power of the turbine.

The electrical losses in the pumped storage system are represented by the efficiency coefficients of the generator and motor. The efficiency of the generator and the motor can be expressed as follows:

$$\eta_{\text{generator}} = \frac{P_{\text{clectric}}}{P_{\text{mechanical}}} \tag{5}$$

$$\eta_{\text{motor}} = \frac{P_{\text{mechanical}}}{P_{\text{electric}}} \tag{6}$$

where P_{clectric} is the electrical power and $P_{\text{mechanical}}$ is the mechanical power.

After detailed modeling of the various types of losses mentioned above, we calculated the overall efficiency of the pumped storage system using a comprehensive efficiency formula. The comprehensive efficiency $\eta_{\text{p-m}}$ is the product of the efficiencies of each component, representing the overall energy conversion efficiency of the entire pumped storage system, specifically:

$$\eta_{\text{p-m}} = \eta_{\text{pump}} \times \eta_{\text{turbine}} \times \eta_{\text{motor}} \times \eta_{\text{generator}} \tag{7}$$

Probability distribution models for distributed power sources are established to address their inherent uncertainty. Wind speed is typically assumed to follow a Weibull distribution, while solar irradiance is assumed to follow a Beta distribution. The probability density function for wind speed is calculated as follows [9]:

$$f(v) = \frac{k}{c}\left(\frac{v}{c}\right)^{k-1} * \exp\left(-\left(\frac{v}{c}\right)^{k}\right) \tag{8}$$

$$k = \left(\frac{\sigma}{\mu}\right)^{-1.086} \tag{9}$$

$$c = \frac{\mu}{\Gamma\left(1+\frac{1}{k}\right)} \tag{10}$$

where v represents the wind speed; k is the shape parameter; and c is the scale parameter.

The probability density function for solar irradiance is calculated as follows:

$$f(G) = \frac{G^{\alpha-1}(1-G)^{\beta-1}}{B(\alpha,\beta)} \tag{11}$$

where G represents the normalized solar irradiance; α and β are the shape parameters; and $B(\alpha,\beta)$ is the Beta parameter.

To capture the variability in power generation, we employ scenario generation techniques to create multiple potential wind and photovoltaic power output scenarios. Each scenario is randomly generated based on different probability distributions, reflecting various weather conditions and time periods.

$$S_i = \left\{P^i_{\text{wind}}(t), P^i_{\text{pv}}(t)\right\},\ i = 1, 2, \ldots, N \tag{12}$$

where S_i represents the i scenario; $P^i_{\text{wind}}(t)$ and $P^i_{\text{pv}}(t)$ represent the output power of wind and photovoltaic generation at time t, respectively; and N is the total number of scenarios.

The probability of each scenario is estimated using historical data, reflecting the likelihood of power generation under different meteorological conditions. By considering these probabilities, we can prioritize high-probability scenarios in the scheduling plan, thereby improving the system's actual operational performance.

To address the complex interactions between wind energy, photovoltaic power generation, pumped storage systems, and the power grid, our model comprehensively considers

the physical and operational coupling relationships among these system components and the grid. Through precise modeling and optimization methods, we ensure the overall stability and efficient operation of the system. To ensure system stability during sudden changes in power supply and demand, this study's system is modeled for voltage and frequency responses to provide short-term capabilities to handle emergencies such as short-circuit faults and sudden load changes. To describe the voltage recovery process following a fault, the voltage response can be modeled as

$$V(t) = V_{\text{prc}} \cdot \exp(-\zeta t) \cdot \cos(\omega_d t + \phi) \tag{13}$$

where V_{prc} represents the pre-fault voltage; ζ is the damping coefficient; ω_d is the damped oscillation frequency; and ω_d is the phase angle.

The frequency response is used to describe the changes in system frequency following a disturbance and is modeled by the following equation:

$$\Delta f(t) = \Delta f_{\max} \cdot \exp(-\psi t) \cdot \cos(\omega_n t) \tag{14}$$

where $\Delta f_{\max}$ represents the maximum frequency deviation; ψ is the damping coefficient; and ω_n is the natural oscillation frequency.

3. Dispatching Model of Combined Wind–Photovoltaic–Pumped Storage System

3.1. Objective Function

Pumped storage power stations can serve as a special power load and also store surplus power in the power system, greatly reducing the curtailment of wind and solar power, ensuring economic benefits while playing an important role in stabilizing the power grid [18]. This paper considers the generation revenue of each component unit and pollutant emissions as penalty costs and establishes a dispatch model aimed at maximizing the total revenue of the combined system. The objective function can be expressed as

$$\max F = \max\left(F_{pwpg} - F_{wp} - F_p - F_g - F_c\right) \tag{15}$$

where F_{pwpg} is the on-grid revenue of the combined system with wind, photovoltaic, and thermal units and pumped storage; F_{wp} is the operating cost of wind and photovoltaic generation; F_p is the pumping cost of the pumped storage unit; F_g is the cost of power generation by the thermal unit; and F_c is the cost of penalties for pollutant discharges.

The on-grid revenue F_{pwpg} of the combined system containing wind, photovoltaic, and thermal units as well as pumped storage can be expressed as

$$\begin{aligned} F_{pwpg} = {} & C_{pv} \times P_{pv}(t) + C_{\text{wind}} \times P_{\text{wind}}(t) + \\ & C_{pump} \times P_{pump}(t) + C_g P_g(t) \end{aligned} \tag{16}$$

where C_{pv} is the photovoltaic feed-in tariff; C_{wind} is the wind power feed-in tariff; C_{pump} is the pumped storage feed-in tariff; C_g is the feed-in tariff of thermal power unit; $P_{pv}(t)$ is the photovoltaic power at the time t; $P_{\text{wind}}(t)$ is wind power at the time t; $P_{pump}(t)$ is the pumped storage power delivered to the power grid at the time t; $P_g(t)$ is the power of thermal power unit at the time t.

The operation costs of wind and photovoltaic power can be expressed as

$$F_{wp} = \sum_{t=1}^{T} \sum_{i=1}^{N_w} C_1 P_{w,i,t} + \sum_{t=1}^{T} \sum_{i=1}^{N_p} C_2 P_{pv,j,t} \tag{17}$$

where C_1 and C_2 are the generation cost factors of wind turbines and photovoltaics; $P_{W,i,t}$ is the electricity generated by the i-th wind turbine at time t; $P_{pv,j,t}$ is the electricity generation of the j-th photovoltaic at time t; N_w is the number of wind turbines; N_p is the number of photovoltaic.

The pumping cost F_p of the pumped storage unit can be expressed as

$$F_p = C_c \times P_{\mathrm{ps}}(t) \tag{18}$$

where C_c is the pumped hydro tariffs for pumped storage; $P_{\mathrm{ps}}(t)$ is the pumping power of pumped storage.

The generation cost F_g of the thermal power unit can be expressed as

$$F_g = \sum_{t=1}^{T} \sum_{j=1}^{N_G} \left\{ \left(a_j P_{\mathrm{G},j,t}^2 + b_j P_{\mathrm{G},j,t} + c_j \right) + S_j y_{j,t} \right\} \tag{19}$$

where $P_{\mathrm{G},j,t}$ is the power generated by the j-th thermal power unit at time t; T is the total duration of the scheduling cycle; N_G is the number of thermal power units; a_j, b_j, and c_j are the generation cost factor for the j-th thermal power unit; S_j and $y_{j,t}$ are start-up costs and start-up status of the j-th thermal power unit.

During the dispatch process, the output of thermal power units with large pollutant emission should be reduced as much as possible and the output of thermal power units with small pollutant emission should be increased. Therefore, the penalty cost considering the pollutant emission of thermal power units F_c can be expressed as [27]

$$F_c = \sum_{t=1}^{T} \sum_{j=1}^{N_G} \left(\alpha_j P_{\mathrm{G},j,t}^2 + \beta_j P_{\mathrm{G},j,t} + \gamma_j \right) \tag{20}$$

where α_j, β_j, and γ_j are the pollutant emission factor for the j-th thermal power unit.

3.2. Constraints

(1) Power balance constraint

The mathematical relationship between thermal power unit, wind turbine, and photovoltaic output and storage charging and discharging power of the combined system can be expressed as

$$\sum_{G \in N_G} P_{\mathrm{G},j,t} + P_{pump}(t) + \sum_{i=1}^{N_w} P_{w,i,t} + \sum_{i=1}^{N_p} P_{pv,j,t} = P_{\mathrm{ps}}(t) + P_L \tag{21}$$

where $P_{\mathrm{G},j,t}$ is the power generated by the j-th thermal power unit at time t; $P_{\mathrm{W},i,t}$ is the power generated by the i-th wind turbine at time t; $P_{pv,j,t}$ is the power generated by the j-th photovoltaic in at time t; $P_{\mathrm{ps}}(t)$ is the pumped storage pumping power; $P_{pump}(t)$ is the power delivered to the grid by pumped storage at time t; P_L is the load power.

(2) Upper and lower limit constraints of wind turbine output:

$$P_{w,\ \min} \le P_{w,i,t} \le P_{w,\ \max} \tag{22}$$

where $P_{w,\ \max}$ and $P_{w,\ \min}$ are the upper and lower limits of wind turbine output.

(3) Upper and lower limit constraints of photovoltaic output:

$$P_{p,\ \min} \le P_{pv,j,t} \le P_{p,\ \max} \tag{23}$$

where $P_{p,\max}$ and $P_{p,\min}$ are the upper and lower limits of photovoltaic output.

(4) Upper and lower limit constraints of thermal power unit output:

$$P_{G,j,min} \le P_{G,j,t} \le P_{G,j,\max} \tag{24}$$

where $P_{G,j,\max}$ and $P_{G,j,min}$ are the upper and lower limits of thermal power unit output.

(5) Climbing constraints of thermal power units:

The power of different thermal power units that can be increased or decreased within a unit time depends on the operational adjustment parameters. Therefore, in terms of the speed of output adjustment for thermal power units, the ramp-up rate of generator output needs to be taken into account [19]. Different thermal power units have different ramp-up rates and cannot excessively increase or decrease output within a unit time. Consequently, ramp-up constraints for various thermal power units must be considered in the dispatch plan, i.e., [23]:

$$P_{G,j,t} - P_{G,j,t-1} \leqslant v_{up,j}(1 - y_{j,t}) + P_{G,j,min} y_{j,t} \tag{25}$$

$$P_{G,j,t-1} - P_{G,j,t} \leqslant v_{down,j}(1 - z_{j,t}) + P_{G,j,min} z_{j,t} \tag{26}$$

$$y_{j,t} - z_{j,t} = I_{j,t} - I_{j,t-1} \tag{27}$$

$$y_{j,t} + z_{j,t} \leqslant 1 \tag{28}$$

where $y_{j,t}$ is the start-up state of the j-th thermal power unit at time t; $z_{j,t}$ is the shut-down state of the j-th thermal power unit at time t; $I_{j,t}$ is the operation state of the j-th thermal power unit at time t; $v_{up,j}$ and $v_{down,j}$ are the upward and downward climb rates of the j-th thermal power unit at time t in the scheduling cycle.

(6) The output constraints of pumped storage unit:

$$P_{pump}^{\min} \le P_{pump}(t) \le P_{pump}^{\max} \tag{29}$$

where $P_{pump}^{\max}$ and $P_{pump}^{\min}$ are the maximum and minimum output of the pumped storage unit, respectively.

(7) The acceptance capacity constraint of power grid:

$$P_{\min} \le P_{pv} + P_w + P_{pump} + P_G \le P_{\max} \tag{30}$$

where $P_{\max}$ and $P_{\min}$ are the upper and lower limits of acceptance capacity of the power grid.

4. Solving Method of Scheduling Model Based on Improved Bat Algorithm

To address the trade-off between maximizing economic benefits and minimizing environmental emissions, this study employs a constraint-based approach to transform the multi-objective problem of balancing pollutant emission costs and economic benefits into a single-objective problem. The maximization of economic benefits is optimized as the overall objective function, with pollutant emissions treated as a constraint. The mathematical formulation is as follows:

$$\max F \quad s.t. \begin{cases} F_c \le \varepsilon \\ (21) - (30) \end{cases} \tag{31}$$

Within the interval [0,1], a fuzzy decision-maker assigns a fuzzy membership degree to each point, with the membership function defined as

$$\hat{f}_k = \begin{cases} 1 & f_k \le f_k^L \\ \frac{f_k^{\max} - f_k}{f_k^{\max} - f_k^{\min}} & f_k^L \le f_k \le f_k^U \\ 0 & f_k \ge f_k^U \end{cases} \tag{32}$$

The optimal compromise solution is obtained using the Min–Max method, where the minimum of the maximum values is selected as the best compromise solution.

Based on the bionic principle of bats, the bat algorithm comprises three elements: the pulse frequency for searching, the pulse intensity, and the pulse emission rate [28,29]. Among these, the speed of flight is determined by the search pulse frequency, while the probability of updating the position after reception is determined by the pulse intensity and the pulse emission rate. The steps of the bat algorithm are as follows:

Step 1: Set the bat population size n Pop, the maximum pulse tone intensity A, the maximum pulse frequency r_0, the upper limit of the pulse frequency $f_{\max}$, the lower limit of the pulse frequency $f_{\min}$, the tone intensity decay coefficient α, and the frequency increase coefficient γ. Set the dimensions of the position vector nVar and the maximum number of iterations MaxIt.

Step 2: Initialize the bat position S_i (i = 1, 2, …, nVar), and at the same time, according to the objective function, the fitness value of the bat position is calculated to find the individual S_{best} in the optimal position. The bat position is initialized as shown in Equation (33).

$$S_i = W_{\min} + (W_{\max} - W_{\min}) \text{ rand } (1, n\text{Var}) \tag{33}$$

where $W_{\max}$ and $W_{\min}$ are the upper and lower limits of the region where the bat is located; rand $(1, n\text{Var})$ is the random generation of a one-dimensional vector matrix containing nVar individual values in the range (0,1).

Step 3: Initialize the pulse frequency of the bat, calculate the flight speed of the bat, and update the position of the bat. The updating equations are shown in Equations (34) and (36).

$$f_i = f_{\min} + (f_{\min} - f_{\max}) \text{ rand} \tag{34}$$

$$v_i^t = v_i^{t-1} + \left(S_i^{t-1} - S_{\text{best}}\right) f_i \tag{35}$$

$$S_i^t = S_i^{t-1} + v_i^t \tag{36}$$

where rand is a random factor, uniformly distributed in the interval (0,1); v_i^{t-1} and v_i^t are the flight speed of the i-th bat at time $t-1$ and t; S_i^{t-1} and S_i^t are the position of the bat.

Step 4: In each iteration, a random number *rand*1 is generated for the bat, and if *rand*1 > r_i^t, the current best solution is selected for local perturbation. Where r_i^t is the pulse frequency of the i-th bat. The local perturbation is shown in Equation (37).

$$S_i^t = S_{\text{best}} + 0.1 * r_i^t * \text{rand } (1, n\text{Var}) \tag{37}$$

Step 5: Calculate the new fitness of the bat after perturbation, if the new fitness is better than its own optimal fitness or *rand* 2 < r_i^t, replace the old position with the new position, and update the pulse frequency and tone intensity at the same time, which are shown in Equations (38) and (39).

$$r_i^{t+1} = r_0[1 - \exp(-\gamma t)] \tag{38}$$

$$A_i^{t+1} = \alpha A_i^t \tag{39}$$

where A_i^t is the impulse sound intensity of the i-th bat; α is the sound intensity attenuation coefficient; r_0 is the maximum impulse frequency; and γ is the frequency increase coefficient.

Step 6: Stop the search when the maximum number of iterations is reached. Output the location and fitness value of the bat correspond to the global optimal solution; otherwise, jump back to Step 3 to continue the search.

With the number of iteration increases for the basic bat algorithm, the individual differences within the population become increasingly large, while the diversity of the population decreases and ultimately tends to zero [30]. Therefore, in the improved bat algorithm, chaotic initialization and the Cauchy function were introduced. The algorithm was enhanced by dynamically adjusting the step size, which accelerated its convergence speed. The Cauchy function improved the algorithm's ability to escape local optima, effectively preventing it from being trapped in suboptimal solutions. Compared to the original algorithm, the improved version exhibits better adaptability to high-dimensional problems. The solution process of the model is shown in Figure 2. The improvement strategies presented below.

A. Population initialization by using chaotic mapping

In the initial stage of the bat algorithm, the population is initialized randomly, which cannot cover the entire solution space. Therefore, this paper adopts the method of chaotic mapping for population initialization to improve the coverage of the initial solution space. The calculation formula is

$$y_i^{k+1} = \left| 1 - 2 \times \left(y_i^k \right)^2 \right| \quad k = 1, 2, \cdots nVar; i = 1, 2, \cdots nPop \tag{40}$$

where $y_i^k \in [0, 1]$ is the chaotic sequence; nVar is the initialized population dimension; nPop is the initialized population number. Perform inverse mapping operation on $y_i^k \in [0, 1]$ to obtain the solution space initialization population pair, and the calculation formula is

$$S_i^k = l_i + (u_i - l_i) y_i^k \tag{41}$$

where l_i and u_i are the minimum and maximum values of the variable, respectively.

B. Adaptive Step Updating

To update the bat speed based on Equations (38) and (39), this paper proposes a bat speed updating method based on adaptive step-size updating. The algorithm starts with a relatively large initial step size to enhance convergence speed, and then reduces the step size in the later stages of the algorithm to achieve refined search results.

$$v_i^{t+1} = \delta_i^t v_i^t + \left(S_i^t - S_{\text{best}} \right) \times r_0 \tag{42}$$

$$\delta_i^t = K \times e^{-10\left(\frac{t}{T_{\max}}\right)^2} + \text{step}_{\min} \tag{43}$$

where $\text{step}_{\min}$ is the minimum step size; $T_{\max}$ is the maximum number of iterations, t is the current number of iterations; and K is the adjustment factor.

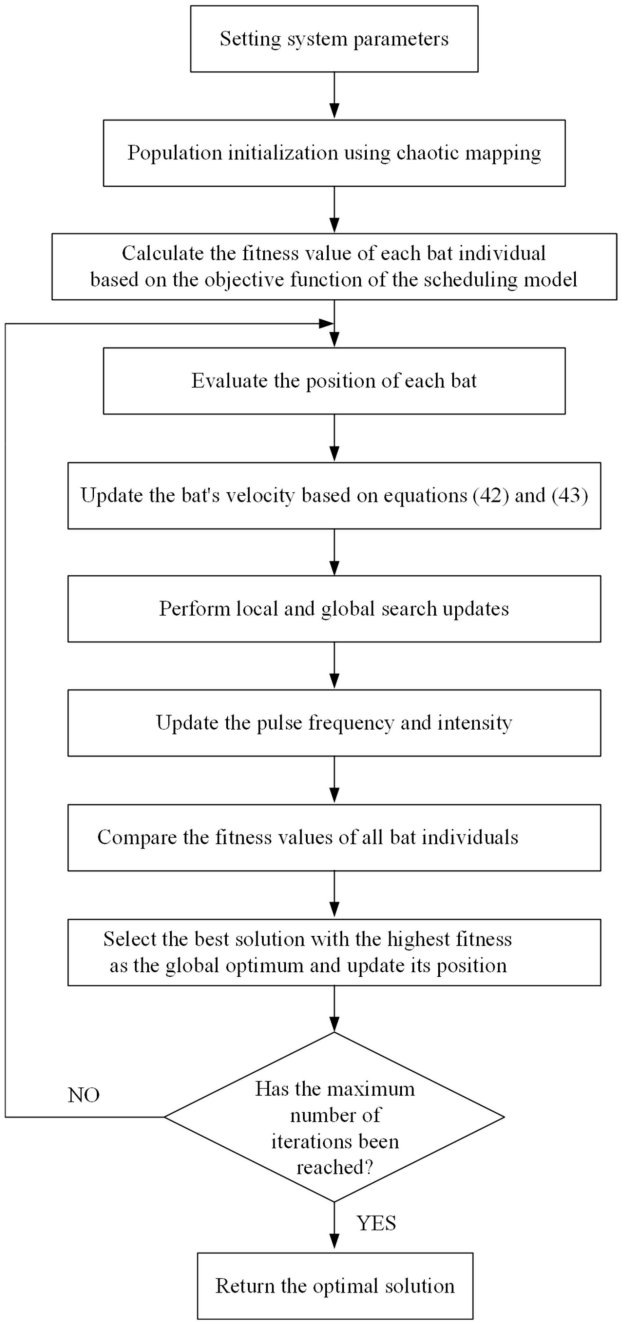


Figure 2. Scheduling model solution process based on improved bat algorithm.

C. Cauchy Mutation Inverse Cumulative Distribution Function

In this paper, the Cauchy mutation inverse cumulative distribution function (hereinafter referred to as the Cauchy function) is introduced into the bat algorithm. Cauchy mutation originates from the Cauchy distribution of continuous probability distributions. This paper employs an appropriate random variable to generate a Cauchy mutation factor, which is used in Step 3 of the bat algorithm. This factor is added to the velocity variable at time t to alter the flight speed of the bats, thereby enhancing the ability to escape local optima. The mutation formula is expressed in Equations (44) and (45).

$$S_i^{t+1} = S_i^t + v_i^{t+1} \cdot \vec{A} \cdot \tan[\pi \cdot (r - 0.5)] \tag{44}$$

$$\vec{A} = 2\vec{a} \cdot \vec{r} \tag{45}$$

where r is a uniformly distributed random number in the interval [0,1]; $\vec{A}$ is a vector of coefficients; $\vec{a}$ is a linearly decreasing vector from 2 to 0; $\vec{r}$ is a uniformly distributed random vector in the interval [0,1].

5. Case Study

Three thermal power units, one pumped storage power plant, one wind farm, and one photovoltaic power plant, are set up in the combined system. This case study aims to balance the complexity of the model with the feasibility of practical applications. To validate the effectiveness of the proposed model and the improved algorithm, some data were selected to reflect the characteristics of real-world power grid operations. The distributed power generation data were referenced from [31], while the parameters for pumped storage equipment were derived from the data in [21]. The installed capacity of each power source is shown in Table 2. The feed-in tariff is shown in Table 3. The parameters of thermal power units are shown in Table 4. The wind power and photovoltaic output curves are shown in Figure 3.

Table 2. Model parameters.

Parameter	Value
Pumped storage unit capacity/MW	300
Upper and lower limits of wind farm output/MW	50.0
Upper and lower limits of PV plant output/MW	20.0
Regulating capacity of pumped storage upper reservoir/m^3	6.25×10^6
Reservoir regulation capacity under pumped storage/m^3	6.20×10^6
Hydraulic turbine power generation efficiency	0.9
Pumping efficiency	0.91

Table 3. Feed-in tariffs.

Type of Power Generation	Feed-in Tariff/USD·MWh
WT	95.4
PV	53.8
Pumped storage	66.2

Table 4. Parameters of thermal power units.

Unit	Output Power Upper Limit/MW	Output Power Lower Limit/MW	Power Generation Cost Factor			Pollutant Emission Factor		
			a_j	b_j	c_j	α_j	β_j	γ_j
G1	275	130	0.002	0.245	42.314	0.012	6.657	654.187
G2	300	160	0.003	0.376	53.541	0.025	2.415	241.361
G3	250	120	0.002	0.245	22.487	0.022	3.547	587.241

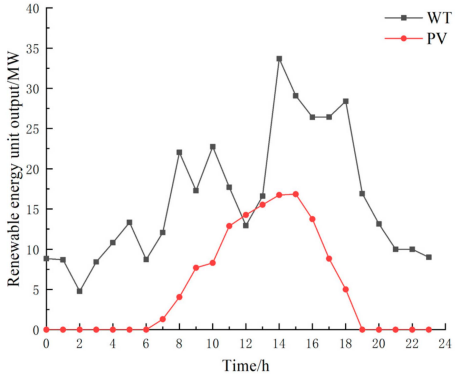


Figure 3. WT and PV output curve.

To validate the robustness of the improved bat algorithm, we applied the bat algorithm, PSO algorithm, and the improved bat algorithm to three typical test functions and tested and compared the results of each algorithm in MATLAB R2016b. The following six test functions are used:

Schaffer function:

$$f_1(x) = 0.5 - \left(\sin\left(\sqrt{\left(x_1^2 + x_2^2\right)^2} - 0.5\right) / \left(1 + 0.01 \cdot \left(x_1^2 + x_2^2\right)\right)^2 \quad (46)$$

Ackley function:

$$f_2(x) = 100 \cdot \left(x_2 - x_1^2\right)^2 + (x_1 - 1)^2 \quad (47)$$

Salomon function:

$$f_3(x) = -\cos\left(2 \cdot p \cdot \sqrt{\sum_{i=1}^{n} x_i^2}\right) + 0.1 \cdot \sqrt{\sum_{i=1}^{n} x_i^2} + 1 \quad (48)$$

For the three different test functions, the maximum number of iterations and population sizes were set to different values, as shown in Table 5.

Table 5. Standard test functions.

Function	Retraction Range	Minimum Value
Schaffer	[−5,5]	1
Ackley	[−15,15]	0
Salomon	[−10,10]	0

For the analysis of the optimal and average optimal values, the specific parameters were set as follows: 200 iterations and a population size of 40. To avoid errors caused by the stochastic nature of the algorithms, each of the three functions was independently run 30 times at different dimensions, and the worst, best, and average values were recorded. The results are shown in Table 6.

Table 6. The optimal value, the worst value, and average optional value of test function.

Test Function.	Dimension	Algorithm	Worst Value	Best Value	Average Value
Schaffer	10	PSO	2.7641	0.0077	0.8541
	10	Bat	0.1278	0.0018	0.0151
	10	Improved bat	0.0036	0.0003	0.0016
Ackley	20	PSO	4.3997	0.0680	3.1437
	20	Bat	0.1776	0.0127	0.0749
	20	Improved bat	0.0818	0.0001	0.0039
Salomon	20	PSO	3.6995	0.0567	2.1489
	20	Bat	0.0477	0.0004	0.0074
	20	Improved bat	0.0013	0.0001	0.00006

From Table 6, it can be seen that compared with the bat and PSO algorithms, the proposed algorithm exhibits better overall optimization performance when solving low-dimensional test functions. The optimal values obtained are closer to the theoretical values, and the algorithm demonstrates good robustness, further indicating that the improved bat algorithm has strong adaptability and robustness.

The bat algorithm, particle swarm algorithm, and improved bat algorithm were used for simulation comparison. The maximum number of iterations of the algorithm was set to 200 and the population size to 100. The convergence curves of the simulation iterations are shown in Figure 4.

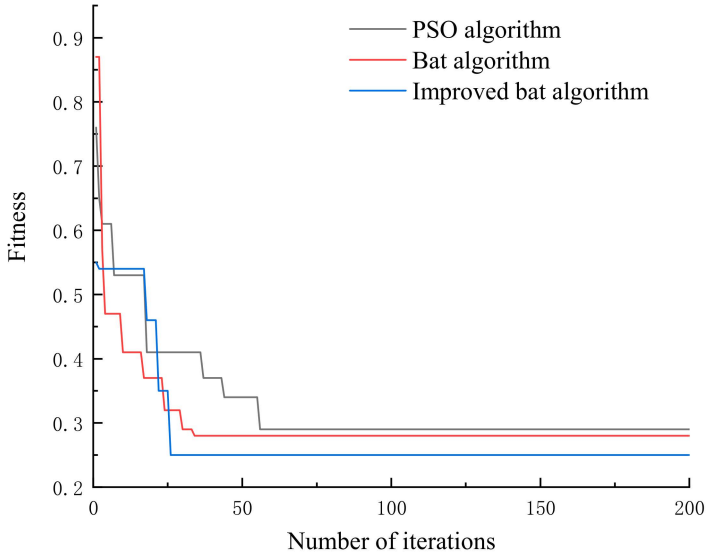


Figure 4. Number of algorithmic iterations.

In Figure 4, it can be seen that the improved bat algorithm adopted in this paper can converge to the optimal solution with fewer iterations in the optimization solving process. Its optimization and solution efficiency are significantly better than the traditional bat algorithm and particle swarm algorithm. Thus, the necessity and effectiveness of the improved bat algorithm for determining optimal scheduling solutions are verified. The revenue curves of the combined system at each moment after using the bat algorithm, particle swarm algorithm, and improved bat algorithm are shown in Figure 5.

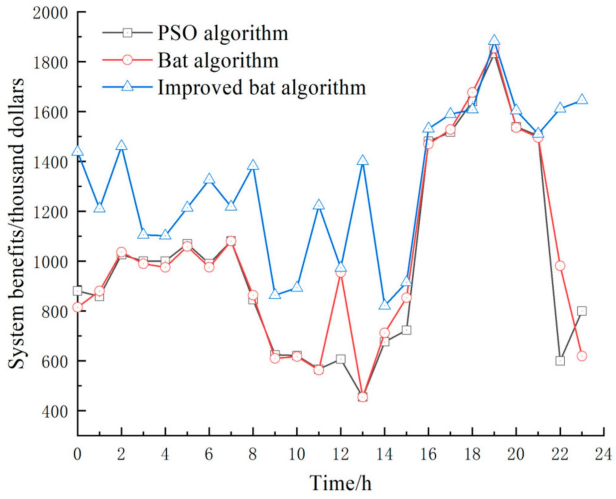


Figure 5. Revenue curve of the co-generation system.

As can be seen from Figure 5, the improved bat algorithm has much higher returns than the original bat algorithm and the improved bat algorithm returns for all time periods up to hour 15. At hour 15 and after the time period, some of the comprehensive gains are lower than from the other two algorithms, but the overall comprehensive gains are slightly higher than those of the other two algorithms. After the final optimization, the bat algorithm improves the overall comprehensive gain by 2.7% compared with the particle swarm algorithm, and the improved bat algorithm improves the overall comprehensive gain by 21.9% compared with the bat algorithm. The results of thermal power unit scheduling based on the method of this paper are shown in Table 7.

Table 7. Day-ahead scheduling results for thermal power units.

Time	Unit G1/MW	Unit G2/MW	Unit G3/MW	Time	Unit G1/MW	Unit G2/MW	Unit G3/MW
1	225.74	272.27	142.53	13	275.00	300.62	179.39
2	222.02	259.07	141.43	14	270.95	297.07	161.95
3	233.17	279.59	152.49	15	273.08	297.31	163.85
4	249.59	285.18	167.39	16	261.07	289.48	164.29
5	250.38	285.65	171.78	17	258.59	287.50	189.00
6	253.59	288.74	176.78	18	275.00	299.34	220.58
7	260.48	291.75	189.45	19	275.00	301.36	235.92
8	267.87	297.28	199.84	20	275.00	300.62	240.00
9	274.07	301.10	229.96	21	275.00	297.98	210.96
10	275.00	300.57	221.42	22	276.17	282.84	201.24
11	275.00	301.42	209.19	23	262.27	278.51	188.75
12	275.00	300.03	190.72	24	250.15	272.07	161.76

As can be seen from Table 7, the change in the output of unit 3 is more sensitive to the introduction of the penalty cost, which is due to the higher pollutant emission factor of this unit. With the introduction of penalty cost, the highest pollutant emission factor of unit 3 will be dispatched less. In this process, thermal power units do not need to adjust the output plan frequently, and the equivalent load of the system is basically unchanged. This not only greatly attenuates the impact of additional shocks to the system caused by traditional large-scale new energy grid integration, but also makes full use of pumped storage power stations, which jointly participate in the system's peak shaving and valley filling tasks in a more rational way.

The Pareto optimal solutions obtained using the constraint method are shown in Figure 6. It can be observed that after 20 iterations, the Pareto optimal solution was reached, with the maximum membership function value being 0.740, corresponding to the 13th solution. Therefore, considering the Min–Max fuzzy satisfaction method, the 13th solution is selected as the best compromise solution.

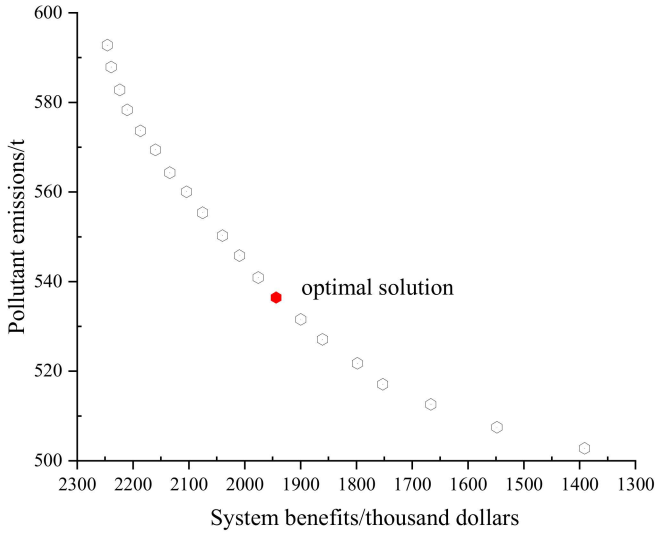


Figure 6. Pareto frontier of multi-objective optimization.

6. Conclusions

The optimization scheduling problem of combined wind–solar–pumped storage systems is investigated in this study, and an optimization scheduling model aimed at maximizing comprehensive revenue is proposed. The issues of traditional methods, such as susceptibility to local optima and low convergence efficiency, are addressed through the

development of an improved bat algorithm. The flexible regulation capabilities of pumped storage are utilized to balance the impact of wind and photovoltaic power fluctuations on grid stability, achieving both economic and environmental benefits. Simulation results demonstrate that the improved bat algorithm significantly outperforms traditional algorithms in terms of optimization efficiency and solution quality. Comprehensive revenue is shown to be substantially enhanced, while reliance on conventional thermal power units is reduced, resulting in lower pollutant emissions. The superiority of the improved algorithm in solving high-dimensional complex optimization problems is validated, providing a novel approach for addressing the scheduling optimization of large-scale energy systems.

As the accuracy of the proposed method depends on factors such as load forecasting and renewable energy output prediction in day-ahead scheduling, improvements in the precision of load forecasts and distributed power output predictions are considered crucial for enhancing the model's accuracy. Future work can focus on several aspects: first, the applicability of the model to large-scale, multi-regional energy systems could be further improved; second, machine learning techniques could be integrated to enhance the accuracy of wind and photovoltaic output predictions, thereby increasing the practicality of scheduling solutions. Additionally, the application of the algorithm in real-time scheduling scenarios could be explored to address the requirements of dynamic load changes and unexpected events.

Author Contributions: Conceptualization, H.F., H.W., S.L., S.H. (Shengfeng Han), J.R., S.H. (Shuo Huang) and H.Z.; software, H.F., H.W., S.L., S.H. (Shengfeng Han), J.R., S.H. (Shuo Huang) and H.Z.; writing—original draft preparation, H.F., H.W., S.L., S.H. (Shengfeng Han), J.R., S.H. (Shuo Huang) and H.Z. All authors have read and agreed to the published version of the manuscript.

Funding: This research received no external funding.

Data Availability Statement: Data are contained within the article.

Conflicts of Interest: Authors Hui Fan, Hongbo Wu and Shilin Li were employed by the company State Grid Hebei Electric Power Co., Ltd. Authors Shengfeng Han and Jingtao Ren were employed by the company State Grid Xingtai Power Supply Co., Ltd. The remaining authors declare that the research was conducted in the absence of any commercial or financial relationships that could be construed as a potential conflict of interest.

References

1. Diaz, H.; Guedes Soares, C. Review of the current status, technology and future trends of offshore wind farms. *Ocean. Eng.* **2020**, *209*, 107381. [CrossRef]
2. Tu, Q.; Miao, S.; Yao, F.; Yang, W.; Lin, Y.; Zheng, Z. An improved wind power uncertainty model for day-ahead robust scheduling considering spatiotemporal correlations of multiple wind farms. *Int. J. Electr. Power Energy Syst.* **2023**, *145*, 108674. [CrossRef]
3. Estupendo, G.F.; Ferreira, F.A.; Govindan, K.; Correia, R.J.; Pereira, L.F.; Meidutė-Kavaliauskienė, I. "Life after coal": Renewable energy impacts on SME conduct. *IEEE Trans. Eng. Manag.* **2023**, *70*, 3571–3586. [CrossRef]
4. Zhang, X.; Ge, S.; Liu, H.; Zhou, Y.; He, X.; Xu, Z. Distributionally robust optimization for peer-to-peer energy trading considering data-driven ambiguity sets. *Appl. Energy* **2023**, *331*, 120436. [CrossRef]
5. Mahmood, H.; Blaabjerg, F. Autonomous power management of distributed energy storage systems in islanded microgrids. *IEEE Trans. Sustain. Energy* **2022**, *13*, 1507–1522. [CrossRef]
6. Tebibel, H. Methodology for multi-objective optimization of wind turbine/battery/electrolyzer system for decentralized clean hydrogen production using an adapted power management strategy for low wind speed conditions. *Energy Convers. Manag.* **2021**, *238*, 114125. [CrossRef]
7. Abomazid, A.M.; El-Taweel, N.A.; Farag He, Z. Optimal energy management of hydrogen energy facility using integrated battery energy storage and solar photovoltaic systems. *IEEE Trans. Sustain. Energy* **2022**, *13*, 1457–1468. [CrossRef]
8. Jiang, Y.; Huang, W.; Yang, G. Electrolysis plant size optimization and benefit analysis of a far offshore wind-hydrogen system based on information gap decision theory and chance constraints programming. *Int. J. Hydrogen Energy* **2022**, *47*, 5720–5732. [CrossRef]

9. Zhai, J.; Jiang, Y.; Shi, Y.; Jones, C.N.; Zhang, X.P. Distributionally robust joint chance-constrained dispatch for integrated transmission-distribution systems via distributed optimization. *IEEE Trans. Smart Grid* **2022**, *13*, 2132–2147. [CrossRef]
10. Li, Y.; Xie, Z.; Yang, S.; Ren, Z. A Hybrid Algorithm Based on NSGA-II and MOPSO for Multi-Objective Designs of Electromagnetic Devices. *IEEE Trans. Magn.* **2023**, *59*, 7001804. [CrossRef]
11. Zhao, Z.; Yang, J.; Yang, W.; Luo, H.; Peng, Y. Coordinated Multi-Objective Optimization for Multiple Trade-Offs in Pumped Outage Condition of Pumped Storage System. *IEEE Access* **2019**, *7*, 161394–161411. [CrossRef]
12. Yan, X.; Zuo, H.; Hu, C. Load Optimization Scheduling of Chip Mounter Based on Hybrid Adaptive Optimization Algorithm. *Complex Syst. Model. Simul.* **2023**, *3*, 1–11. [CrossRef]
13. Fakhar, M.S. Implementation of APSO and Improved APSO on Non-Cascaded and Cascaded Short Term Hydrothermal Scheduling. *IEEE Access* **2021**, *9*, 77784–77797. [CrossRef]
14. Li, J.; Fang, Z.; Wang, Q.; Zhang, M.; Li, Y.; Zhang, W. Optimal Operation with Dynamic Partitioning Strategy for Centralized Shared Energy Storage Station with Integration of Large-scale Renewable Energy. *J. Mod. Power Syst. Clean Energy* **2024**, *12*, 359–370. [CrossRef]
15. Lu, Y.; Jiang, T. Bi-Population Based Discrete Bat Algorithm for the Low-Carbon Job Shop Scheduling Problem. *IEEE Access* **2019**, *7*, 14513–14522. [CrossRef]
16. Khan, Z.A.; Aziz, I.A.; Osman, N.A.B.; Ullah, I. A Review on Task Scheduling Techniques in Cloud and Fog Computing: Taxonomy, Tools, Open Issues, Challenges, and Future Directions. *IEEE Access* **2023**, *11*, 143417–143445. [CrossRef]
17. Dong, Z.; Tan, J.; Muljadi, E.; Nelms, R.M.; St-Hilaire, A.; Pevarnik, M.; Jacobson, M.D. Developing of Quaternary Pumped Storage Hydropower for Dynamic Studies. *IEEE Trans. Sustain. Energy* **2020**, *11*, 2870–2878. [CrossRef]
18. Bao, L.; He, Z.; Tan, J.; Chen, Y.; Zhao, M. Thermal-Aware Task Scheduling and Resource Allocation for UAV-and-Basestation Hybrid-Enabled MEC Networks. *IEEE Trans. Green Commun. Netw.* **2023**, *7*, 579–593. [CrossRef]
19. Yang, L.; Li, H.; Zhang, H.; Wu, Q.; Cao, X. Stochastic-Distributionally Robust Frequency-Constrained Optimal Planning for an Isolated Microgrid. *IEEE Trans. Sustain. Energy* **2024**, *15*, 2155–2169. [CrossRef]
20. Senthilnath, J.; Kulkarni, S.; Benediktsson, J.A.; Yang, X.S. A Novel Approach for Multispectral Satellite Image Classification Based on the Bat Algorithm. *IEEE Geosci. Remote Sens. Lett.* **2016**, *13*, 599–603. [CrossRef]
21. Ghanem, W.A.; Ghaleb, S.A.; Jantan, A.; Nasser, A.B.; Saleh, S.A.; Ngah, A.; Alhadi, A.C.; Arshad, H.; Saad, A.M.; Omolara, A.E.; et al. Cyber Intrusion Detection System Based on a Multiobjective Binary Bat Algorithm for Feature Selection and Enhanced Bat Algorithm for Parameter Optimization in Neural Networks. *IEEE Access* **2022**, *10*, 76318–76339. [CrossRef]
22. Chandrasekaran, G.; Kumar, N.S.; Karthikeyan, P.R.; Vanchinathan, K.; Priyadarshi, N.; Twala, B. Test Scheduling and Test Time Minimization of System-on-Chip Using Modified BAT Algorithm. *IEEE Access* **2022**, *10*, 126199–126216. [CrossRef]
23. Qi, Z.; Zhang, R. Coordinated Scheduling of Micro-Grid Combined Heat and Power Based on Dynamic Feedback Correction and Virtual Penalty Cost. *IEEE Trans. Power Syst.* **2024**, *39*, 4975–4986. [CrossRef]
24. Zhou, Y.; Lu, C.; Zhang, M.; Chen, X.; Wu, M.; Cao, W. A Novel Rate of Penetration Model Based on Support Vector Regression and Modified Bat Algorithm. *IEEE Trans. Ind. Inform.* **2023**, *19*, 6659–6668. [CrossRef]
25. Liu, J.; Wu, Y. An Improved Lion Swarm Optimization Algorithm With Chaotic Mutation Strategy and Boundary Mutation Strategy for Global Optimization. *IEEE Access* **2022**, *10*, 131264–131302. [CrossRef]
26. Ma, G.; Yan, N.; Wang, M.; Li, X.; Ma, S. Multi-Objective Optimization Scheduling of Integrated Energy System Based on Operational Characteristics Clustering. *IEEE Trans. Appl. Supercond.* **2024**, *34*, 3801905. [CrossRef]
27. Ogunwole, E.I.; Krishnamurthy, S. Transmission Congestion Management Using Generator Sensitivity Factors for Active and Reactive Power Rescheduling Using Particle Swarm Optimization Algorithm. *IEEE Access* **2022**, *10*, 122882–122900. [CrossRef]
28. Yang, Y.; Yang, P.; Zhao, Z.; Tang, Y.; Lai, L.L. An Adaptive Optimal Scheduling Strategy for Islanded Micro-Energy Grid Considering the Multiple System Operating States. *IEEE Trans. Sustain. Energy* **2023**, *14*, 393–408. [CrossRef]
29. Zhang, H.; Tian, Y. Coordinated Optimal Scheduling of WPHTNS Power System Based on Adaptive Improved Genetic Algorithm. *IEEE Access* **2023**, *11*, 95600–95615. [CrossRef]
30. Zhu, S.; Wang, E.; Han, S.; Ji, H. Optimal Scheduling of Combined Heat and Power Systems Integrating Hydropower-Wind-Photovoltaic-Thermal-Battery Considering Carbon Trading. *IEEE Access* **2024**, *12*, 98393–98406. [CrossRef]
31. Chazarra, M.; Pérez-Díaz, J.I.; García-González, J. Optimal Joint Energy and Secondary Regulation Reserve Hourly Scheduling of Variable Speed Pumped Storage Hydropower Plants. *IEEE Trans. Power Syst.* **2018**, *33*, 103–115. [CrossRef]

Disclaimer/Publisher's Note: The statements, opinions and data contained in all publications are solely those of the individual author(s) and contributor(s) and not of MDPI and/or the editor(s). MDPI and/or the editor(s) disclaim responsibility for any injury to people or property resulting from any ideas, methods, instructions or products referred to in the content.